

# Expanding element interpolation method for analysis of thin-walled structures

Jianming Zhang\*, Yudong Zhong, Yunqiao Dong, Weicheng Lin

*State Key Laboratory of Advanced Design and Manufacturing for Vehicle Body, College of Mechanical and Vehicle Engineering, Hunan University, Changsha 410082, China*

Correspondence to: Jianming Zhang

College of Mechanical and Vehicle Engineering, Hunan University, Changsha 410082, China

Telephone: +86-731-88823061

E-mail: zhangjm@hnu.edu.cn

## Abstract

An expanding element is obtained by adding virtual nodes along the perimeter of the traditional discontinuous element. There are two kinds of shape functions in the expanding element: (i) the raw shape function, i.e. shape function of the original discontinuous element, involving only inner nodes; (ii) the fine shape function, which involves all the nodes including inner nodes and the newly added virtual nodes. The polynomial order of fine shape functions of the expanding elements increases by two compared with their corresponding raw shape functions. In this paper, we apply the expanding element interpolation method to analysis of thin-walled structures. An adaptive element subdivision method for evaluating nearly singular integrals is proposed. Numerical results have demonstrated that our method has high level of accuracy and is able to analyze very slender structures with the aspect ratio up to  $1e6$ .

**Keywords:** thin-walled structures; nearly singular integrals; expanding element interpolation method; boundary element method

## 1. Introduction

Thin-walled structures, such as various thin films in electronic devices, sensors and actuators in smart materials, and coatings on machine components, widely appear in engineering application. Accurate and efficient numerical analysis of these structures has been a challenging task. The finite element method (FEM) is a successful tool to

analyze the thin-walled structures using plate and shell elements in most applications. But the plate and shell elements are based on plate and shell theories in which many assumptions about the geometry, loading and deformation of structure are introduced. While using brick elements in the FEM, large number of elements are required due to the aspect ratio limitations of the elements.

The boundary element method (BEM) [1-8] is a more suitable method for numerical analysis of thin-walled structures. This is because, in BEM analysis, only the surface of a body needs to be discretized and accurate results for stress can be obtained without shell assumption. This is particularly beneficial when dealing with connections between thin-walled parts and bulky blocks within a complicated structure. In addition, the trial functions in the FEM formulation must be at least  $C^0$ -continuous which is not required in the BEM. This feature is significantly important for the BEM to be superior to the FEM. However, how to make full use of this feature has been a long-standing issue in the BEM community [9], because the continuous and discontinuous elements each have their own advantages and disadvantages.

When using the discontinuous elements, many advantages are provided, for example, simplifying the assembly of the system equations, the mesh generation and the computation of the 'free' terms appearing in the integral equations. But for the same level of accuracy, the number of degrees of freedom is larger, thus more CPU time and memory capacity are required. For the continuous elements, the  $C^0$  continuity can be guaranteed, but not the  $C^1$  continuity which is necessary for hypersingular integral equation [10, 11]. In addition, the corner problems [12] must be considered when using the continuous elements.

To unify the continuous and discontinuous elements, a new expanding element is presented. The expanding element is achieved by adding virtual nodes along the perimeter of the traditional discontinuous element. The inner nodes of discontinuous element are called as source nodes. The boundary integral equation is collocated at the source node, only. There are two kinds of shape functions in the expanding element: the raw shape function and the fine shape function. The raw shape functions are used

to build relationship between the virtual nodes and source nodes. While the fine shape functions are used for interpolating boundary field variables. With the expanding element, both continuous and discontinuous fields on the domain boundary can be accurately approximated, and the interpolation accuracy increases by two orders compared with the original discontinuous element.

In this paper, we apply the expanding element interpolation method to analyze thin-walled structures. Accurate and efficient evaluation of nearly singular integrals is of crucial importance for solving thin structures problems. Various methods have been proposed to cope with nearly singular integrals, such as element subdivision method [13, 14], analytical and semi-analytical method [15], exponential transformation [16, 17], distance transformation [18, 19] and sinh transformation [20-22]. Among these methods, the element subdivision method is a more stable and universal method. An adaptive element subdivision method for evaluating nearly singular integrals is proposed in this paper. In this method, the integration element is divided into two equal sub-elements according to the location of the source node, and it is performed in local coordinate system of the element. With the proposed method, the nearly singular integrals can be accurately evaluated even when the source node is very close to the integration element. Furthermore, this method is independent of the problem to be solved.

This paper is organized as follows. Section 2 presents the expanding element interpolation method. In section 3, the assembly of the system of linear algebraic equations and the nearly singular integration scheme are described. Numerical examples are given in Section 4. The paper ends with conclusions in Section 5.

## **2. The expanding element interpolation method**

The expanding element interpolation method is introduced in detail in this section.

### *2.1 The expanding elements*

The expanding element is obtained by collocating virtual nodes along the perimeter of the traditional discontinuous element as shown in Fig. 1. There are two

kinds of shape functions in the expanding element: raw shape function and fine shape function. The raw shape function is the shape function of the original discontinuous element. The fine shape function is constructed by the virtual nodes and the inner nodes of the discontinuous element. **The raw shape functions and fine shape functions of the expanding constant, linear and quadratic element are as follows:**

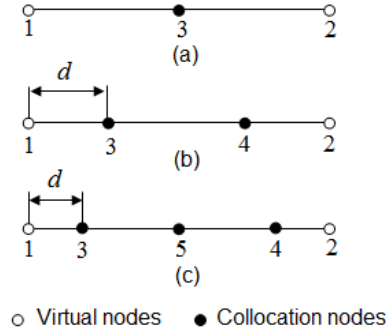


**Fig. 1.** (a) Expanding constant element; (b)expanding linear element; (c) expanding quadratic element.

$$\begin{cases} N_3^r = 1 \\ N_1^f = -0.5\xi(1-\xi) \\ N_2^f = 0.5\xi(1+\xi) \\ N_3^f = (1-\xi)(1+\xi) \end{cases} \quad (1)$$

$$\begin{cases} N_3^r = -\frac{[\xi - (1-d)]}{2(1-d)} \\ N_4^r = \frac{[\xi + (1-d)]}{2(1-d)} \\ N_1^f = -\frac{[\xi + (1-d)][\xi - (1-d)](\xi - 1)}{2d(2-d)} \\ N_2^f = \frac{[\xi + (1-d)][\xi - (1-d)](\xi + 1)}{2d(2-d)} \\ N_3^f = \frac{[\xi - (1-d)](\xi + 1)(\xi - 1)}{2d(1-d)(2-d)} \\ N_4^f = -\frac{[\xi + (1-d)](\xi + 1)(\xi - 1)}{2d(1-d)(2-d)} \end{cases} \quad (2)$$

$$\left\{ \begin{array}{l} N_3^r = \frac{\xi[\xi - (1-d)]}{2(1-d)^2} \\ N_4^r = \frac{\xi[\xi + (1-d)]}{2(1-d)^2} \\ N_5^r = -\frac{[\xi + (1-d)][\xi - (1-d)]}{(1-d)^2} \\ N_1^f = \frac{[\xi + (1-d)][\xi - (1-d)](\xi - 1)\xi}{2d(2-d)} \\ N_2^f = \frac{[\xi + (1-d)][\xi - (1-d)](\xi + 1)\xi}{2d(2-d)} \\ N_3^f = -\frac{[\xi - (1-d)](\xi + 1)(\xi - 1)\xi}{2d(2-d)(1-d)^2} \\ N_4^f = -\frac{[\xi + (1-d)](\xi + 1)(\xi - 1)\xi}{2d(2-d)(1-d)^2} \\ N_5^f = \frac{[\xi + (1-d)][\xi - (1-d)](\xi + 1)(\xi - 1)}{(1-d)^2} \end{array} \right. \quad (3)$$

where  $N$  with the superscripts  $r$  and  $f$  refer to the raw and fine shape functions of the expanding elements, respectively.

The fine shape functions are used for interpolating boundary field variables. From Eqs. (1)-(3), it can be seen that the interpolation accuracy increases by two orders compared with the original discontinuous element. The relationships between the virtual nodes and source nodes are built up by the raw shape functions.

## 2.2 New interpolation method by the expanding element

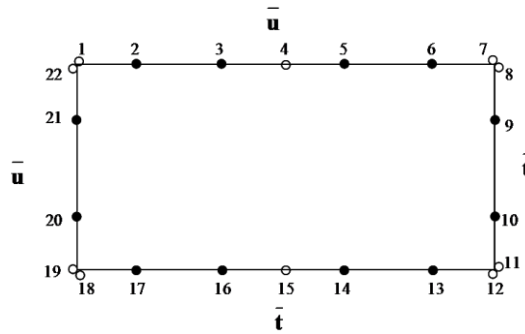


**Fig. 2.** Example of new interpolation method by the expanding linear elements.

Because virtual nodes are not used as source nodes, how to get the nodal values of virtual nodes is very crucial for the implementation of the new method. In the

following example, the calculation of values at virtual nodes is described in detail.

Fig. 2 shows a rectangular domain discretized by 6 expanding linear elements with 12 source nodes and 10 virtual nodes. These elements are used to interpolate displacements and tractions on the boundary.  $\bar{\mathbf{u}}$  and  $\bar{\mathbf{t}}$  in Fig. 2 represent the known displacements and tractions, respectively.

For interpolating known boundary variables with the expanding elements, the nodal values of virtual nodes equal to the corresponding boundary conditions. For instance,  $\mathbf{u}_4 = \bar{\mathbf{u}}_4$  in Fig. 2. Thus, more accurate boundary conditions can be imposed. This is particularly beneficial when dealing with thin-walled structures with short edges.

When interpolating unknown boundary variables, the nodal values of virtual nodes equal to the average of extrapolation values by the raw shape functions of their connecting elements. Taking  $\mathbf{t}_4$  in Fig. 2 for example,

$$\mathbf{t}_4 = \frac{1}{2} \left[ N_2^r(1)\mathbf{t}_2 + N_3^r(1)\mathbf{t}_3 + N_5^r(-1)\mathbf{t}_5 + N_6^r(-1)\mathbf{t}_6 \right] \quad (4)$$

where  $N_2^r$ ,  $N_3^r$ ,  $N_5^r$  and  $N_6^r$  are the raw shape functions of the two expanding linear elements on the top edge. With this scheme, the interelement continuity can be guaranteed.

In order to accurately approximate the discontinuous fields (tractions) on the domain boundary, two virtual nodes are collocated at a vertex geometrically shared by two adjacent elements, one virtual node for one element, respectively. As shown in Fig. 2,

$$\mathbf{t}_7 = \bar{\mathbf{t}}_7, \quad \mathbf{t}_8 = \bar{\mathbf{t}}_8 \quad (5)$$

$$\mathbf{t}_{11} = \bar{\mathbf{t}}_{11}, \quad \mathbf{t}_{12} = \bar{\mathbf{t}}_{12} \quad (6)$$

With this method, the discontinuity of the boundary variables can also be accurately maintained. For continuous fields (displacements), the following scheme is adopt:

$$\mathbf{u}_7 = \mathbf{u}_8 = \bar{\mathbf{u}}_7 \quad (7)$$

$$\mathbf{u}_{11} = \mathbf{u}_{12} = \frac{1}{2} \left[ N_9^r(1)\mathbf{u}_9 + N_{10}^r(1)\mathbf{u}_{10} + N_{13}^r(-1)\mathbf{u}_{13} + N_{14}^r(-1)\mathbf{u}_{14} \right]. \quad (8)$$

The boundary variables are interpolated by the fine shape functions of expanding elements. The displacements and tractions on the right edge in Fig. 2 are

$$\mathbf{u} = N_8^f \mathbf{u}_8 + N_9^f \mathbf{u}_9 + N_{10}^f \mathbf{u}_{10} + N_{11}^f \mathbf{u}_{11} \quad (9)$$

$$\mathbf{t} = N_8^f \mathbf{t}_8 + N_9^f \mathbf{t}_9 + N_{10}^f \mathbf{t}_{10} + N_{11}^f \mathbf{t}_{11} \quad (10)$$

Substituting Eqs. (5)-(8) into Eqs. (9) and (10), the following expressions can be obtained.

$$\begin{aligned} \mathbf{u} = & N_8^f \bar{\mathbf{u}}_7 + \left[ N_9^f + \frac{1}{2} N_{11}^f N_9^r(1) \right] \mathbf{u}_9 + \left[ N_{10}^f + \frac{1}{2} N_{11}^f N_{10}^r(1) \right] \mathbf{u}_{10} \\ & + \frac{1}{2} N_{11}^f N_{13}^r(-1) \mathbf{u}_{13} + \frac{1}{2} N_{11}^f N_{14}^r(-1) \mathbf{u}_{14} \end{aligned} \quad (11)$$

$$\mathbf{t} = N_8^f \bar{\mathbf{t}}_8 + N_9^f \bar{\mathbf{t}}_9 + N_{10}^f \bar{\mathbf{t}}_{10} + N_{11}^f \bar{\mathbf{t}}_{11} \quad (12)$$

In the expanding element, the nodal values of virtual nodes are not independent variables. They are either directly used when the boundary condition at the node is known, or interpolated by raw shape functions of their connecting elements. The boundary integral equations are collocated at source nodes, and the size of the final system of linear equations equals to the total number of degrees of freedom counted for source nodes, only. By arranging two virtual nodes at a vertex geometrically shared by two adjacent elements, both continuous and discontinuous fields on the domain boundary can be accurately approximated.

### 3. Solution of boundary integral equations with the expanding element interpolation method

#### 3.1 Assembly of the system of linear algebraic equations

The following boundary integral equation (BIE) for 2D elastostatic problem is considered:

$$c_{ij}(P)u_j(P) = \int_{\Gamma} u_{ij}^*(P, Q)t_j(Q)d\Gamma(Q) - \int_{\Gamma} t_{ij}^*(P, Q)u_j(Q)d\Gamma(Q) \quad (13)$$

where  $P$  and  $Q$  are the source and field node, respectively.  $c_{ij}(P)$  is a coefficient matrix depending on the smoothness of the boundary  $\Gamma$  at the source node  $P$ .  $u_j$  and  $t_j$  represent the displacement and traction fields, respectively. The Kelvin fundamental

solutions  $u_{ij}^*(P, Q)$  and  $t_{ij}^*(P, Q)$  for plane strain problems are given by

$$u_{ij}^*(P, Q) = \frac{1}{8\pi\mu(1-\nu)} \left[ (3-4\nu)\delta_{ij} \ln \frac{1}{r} + r_i r_j \right] \quad (14)$$

$$t_{ij}^*(P, Q) = -\frac{1}{4\pi(1-\nu)r} \left\{ \frac{\partial r}{\partial n} \left[ (1-2\nu)\delta_{ij} + 2r_i r_j \right] - (1-2\nu)(r_i n_j - r_j n_i) \right\} \quad (15)$$

where  $\mu$  and  $\nu$  are the shear modulus and the Poisson's ratio, respectively.  $r$  is the distance between the source node and field node.  $n_i$  and  $n_j$  are the directional cosines of the normal  $n$ .

Eq. (13) is discretized with  $n_e$  expanding elements. The discretized BIE can be expressed as

$$c_{ij}(P)u_j(P) = \sum_{e=1}^{n_e} \left\{ \sum_{\alpha=1}^{n_\alpha} t_j^\alpha \int_{\Gamma_e} u_{ij}^*(P, Q) N_\alpha^f(Q) d\Gamma(Q) \right\} - \sum_{e=1}^{n_e} \left\{ \sum_{\alpha=1}^{n_\alpha} u_j^\alpha \int_{\Gamma_e} t_{ij}^*(P, Q) N_\alpha^f(Q) d\Gamma(Q) \right\} \quad (16)$$

where  $n_\alpha$  is the number of element nodes (including the source and virtual nodes).  $N_\alpha^f$  is the fine shape function of the  $\alpha^{\text{th}}$  node of expanding element. The system of linear algebraic equations can be expressed in matrix form as

$$\mathbf{H}\mathbf{u} = \mathbf{G}\mathbf{t} \quad (17)$$

where vectors  $\mathbf{u}$  and  $\mathbf{t}$  consist of all nodal displacement and traction. Matrix  $\mathbf{H}$  contains integrals involving  $t_{ij}^*$ , and matrix  $\mathbf{G}$  contains integrals involving  $u_{ij}^*$ .

$$\mathbf{H}_{ij} = \int_{\Gamma_e} \mathbf{t}^*(P^i, Q) N_j^f(Q) d\Gamma(Q) \quad (18)$$

$$\mathbf{G}_{ij} = \int_{\Gamma_e} \mathbf{u}^*(P^i, Q) N_j^f(Q) d\Gamma(Q) \quad (19)$$

There are  $n$  source nodes. Distinguishing the known and unknown boundary variables, Eq. (17) can be rewritten as

$$\begin{bmatrix} \bar{\mathbf{H}}^s & \mathbf{H}^s & \bar{\mathbf{H}}^v & \mathbf{H}^v \end{bmatrix} \begin{bmatrix} \bar{\mathbf{u}}^s \\ \mathbf{u}^s \\ \bar{\mathbf{u}}^v \\ \mathbf{u}^v \end{bmatrix} = \begin{bmatrix} \mathbf{G}^s & \bar{\mathbf{G}}^s & \mathbf{G}^v & \bar{\mathbf{G}}^v \end{bmatrix} \begin{bmatrix} \mathbf{t}^s \\ \bar{\mathbf{t}}^s \\ \mathbf{t}^v \\ \bar{\mathbf{t}}^v \end{bmatrix} \quad (20)$$

where  $\bar{\mathbf{u}}^s$ ,  $\bar{\mathbf{t}}^s$  and  $\mathbf{u}^s$ ,  $\mathbf{t}^s$  are the known and unknown boundary variables at the

source nodes, respectively.  $\bar{\mathbf{u}}^v$ ,  $\bar{\mathbf{t}}^v$  and  $\mathbf{u}^v$ ,  $\mathbf{t}^v$  represent the known and unknown boundary variables at the virtual nodes, respectively.

The matrices  $\mathbf{H}$  and  $\mathbf{G}$  are no longer square matrix since the virtual nodes are not used as the source nodes. However, from Section 2.2, we can know that  $\mathbf{u}^v$  and  $\mathbf{q}^v$  are not truly independent variables. They are interpolated by raw shape functions of their connecting elements and can be expressed by the following form:

$$\begin{aligned}\mathbf{u}^v &= \mathbf{N}^r \mathbf{u}^s \\ \mathbf{q}^v &= \mathbf{N}^r \mathbf{q}^s\end{aligned}\quad (21)$$

where  $\mathbf{N}^r$  is the raw shape functions of the expanding element. Substituting Eq. (21) into Eq. (20) and rearranging Eq. (20) according to the boundary conditions, the final system of linear equations can be obtained.

$$\mathbf{A}\mathbf{x} = \mathbf{f} \quad (22)$$

where

$$\mathbf{A} = \begin{bmatrix} \mathbf{H}^s + \mathbf{H}^v \mathbf{N}^r & -(\mathbf{G}^s + \mathbf{G}^v \mathbf{N}^r) \end{bmatrix} \quad (23)$$

$$\mathbf{x} = \begin{bmatrix} \mathbf{u}^s \\ \mathbf{q}^s \end{bmatrix} \quad (24)$$

$$\mathbf{f} = \left[ \bar{\mathbf{G}}^s \bar{\mathbf{q}}^s + \bar{\mathbf{G}}^v \bar{\mathbf{q}}^v - \bar{\mathbf{H}}^s \bar{\mathbf{u}}^s - \bar{\mathbf{H}}^v \bar{\mathbf{u}}^v \right] \quad (25)$$

Matrix  $\mathbf{A}$  matrix is a square matrix of order  $n$ .  $\mathbf{x}$  is the vector containing  $n$  boundary unknowns at the source nodes, only.  $\mathbf{f}$  is the known vector on the right-hand side.

From Eqs. (22)-(25), it can be seen that the size of the overall system of linear equations is just the same as that in the traditional discontinuous element implementation. The variables at the virtual nodes do not appear in the overall system of equations.

### 3.2 Nearly singular integration scheme

The boundary integrals in Eqs. (18) and (19) become nearly singular integrals when the source node  $P$  is close to but not on the element of integration. To provide a general approach, we proposed an integration scheme based on adaptive element subdivision method [13, 14]. In this scheme, we first calculate the length of

integration element,  $l$ , and the distance between the source node and the center of element,  $d$ , in the global coordinate system. If  $l$  is smaller than  $d$ , this element is taken as a regular integration element, or it is divided into two equal sub-elements in local coordinate system as shown in Fig. 3. Then for each sub-element, we repeat the above procedure until all sub-elements become regular. Finally, Gaussian quadrature is used on all sub-elements. With the proposed method, the nearly singular integrals can be accurately evaluated even when the source node is very close to the integration element.

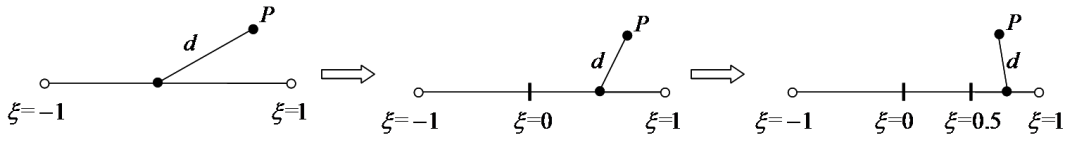


**Fig. 3.** Subdivision of element in local coordinate system according to the position of source node  $P$ .

#### 4. Numerical examples

To verify the accuracy and efficiency of expanding element interpolation method for thin-walled structures, four test examples are presented in this section, together with comparisons with exact solutions. For the purpose of error estimation and convergence studies, a relative errors  $e$  is defined as

$$e = \frac{1}{|u|_{\max}} \sqrt{\frac{1}{N} \sum_{i=1}^N (u_i^{\text{num}} - u_i^{\text{exact}})^2} \quad (26)$$

where  $|u|_{\max}$  is the maximum value over  $N$  sample points.  $u_i^{\text{num}}$  and  $u_i^{\text{exact}}$  stand for the numerical and exact solutions, respectively.

In all following figures,  $n$  is the number of the source nodes. ‘ExpandConst’, ‘ExpandLinear’, ‘ExpandQuad’, ‘DiscontConst’, ‘DiscontLinear’, ‘DiscontQuad’, ‘ContinuLinear’ and ‘ContinuQuad’ denote the numerical results obtained by the expanding constant, linear, quadratic element interpolation methods, traditional discontinuous constant, linear, quadratic element interpolation methods, and traditional continuous linear, quadratic element interpolation methods, respectively.

#### 4.1 Example 1: displacement field problem on an ellipse

A displacement field problem on an ellipse, centered at the origin is concerned in this example as shown in Fig. 4. The semi-major axis  $a$  is kept constant, while the semi-minor axis  $b$  varies from  $a$  to  $10^{-6}a$ . Plane strain cases with Young's modulus  $E = 1$  (in consistent units) and Poisson's ratio  $\nu = 0.25$  are considered for various ratios  $b/a$ . A planar displacement profile is prescribed on the boundary as follows:

$$u_x = y^3 - 3yx^2, \quad u_y = -x^3 + 3xy^2 \quad (27)$$

There are 120 source nodes used in all methods. The relative errors of tractions  $t_x$  along the whole boundary by the expanding elements and traditional elements interpolation method are shown in Fig. 5. To study the convergence, different numbers of source nodes are used for  $b/a = 0.1$  as shown in Fig. 6.

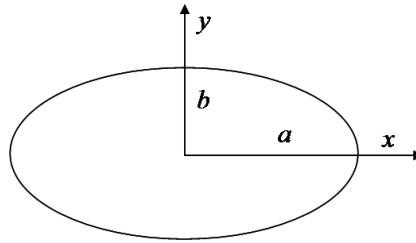


Fig. 4. Displacement field problem on an ellipse.

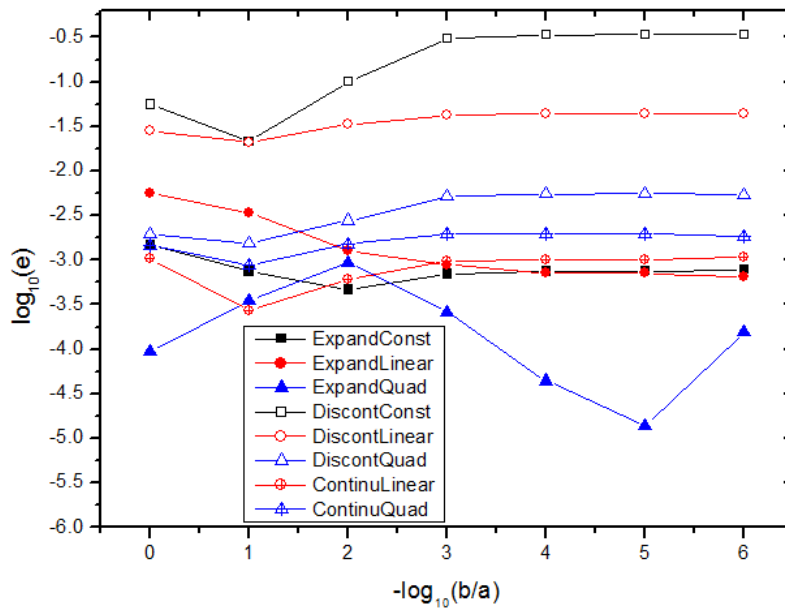
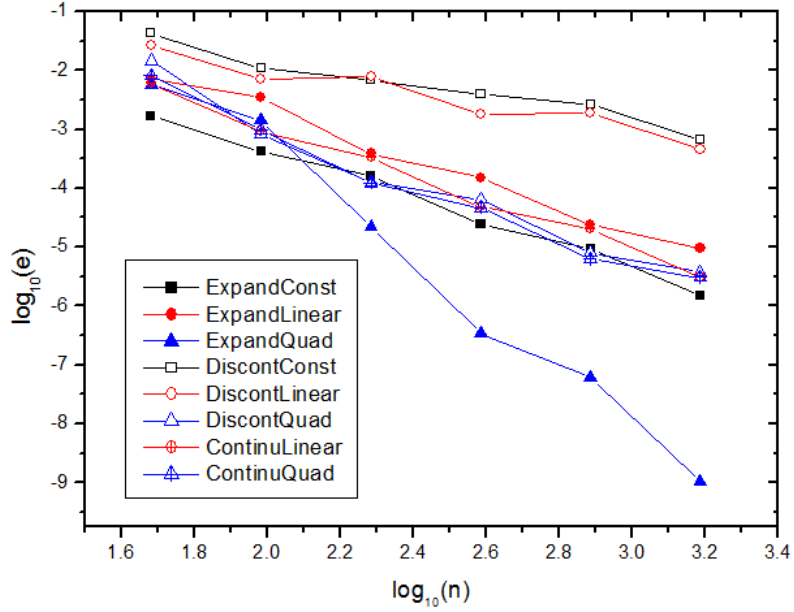


Fig. 5. Relative errors of tractions  $t_x$  along the whole boundary for different ratios  $b/a$ .



**Fig. 6.** Convergence rates of  $t_x$  along the whole boundary for  $b/a = 0.1$ .

From Fig. 5 and 6, it can be seen that the accuracy of expanding elements interpolation method remains very high even for the ratio  $b/a$  in the micro-scale and high convergence rates can be obtained.

#### 4.2 Example 2: displacement field problem on concentric circles

When analyzing a thin coating on a shaft, the geometry model can be simplified into two concentric circles as shown in Fig. 7. The outer radii of two circles are  $r_1$  and  $r_2$ , respectively. The thickness  $h = r_2 - r_1$  varies in the range of  $10^{-1}r_1 - 10^{-6}r_1$ . Essential boundary conditions of Eq. (27) are prescribed on the all boundaries. Plane strain conditions with Young's modulus  $E = 1$  (in consistent units) and Poisson's ratio  $\nu = 0.25$  are assumed. 60 source nodes are used on the inner circle and outer circle, respectively. The relative errors of  $t_y$  along the inner circle by different methods are shown in Fig. 8 and the convergence rates of  $t_y$  for the ratios  $h/r_1 = 10^{-6}$  are shown in Fig. 9.

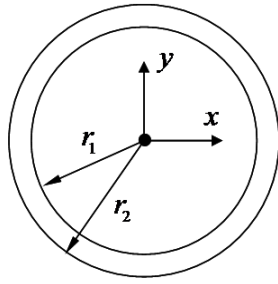


Fig. 7. Displacement field problem on concentric circles.

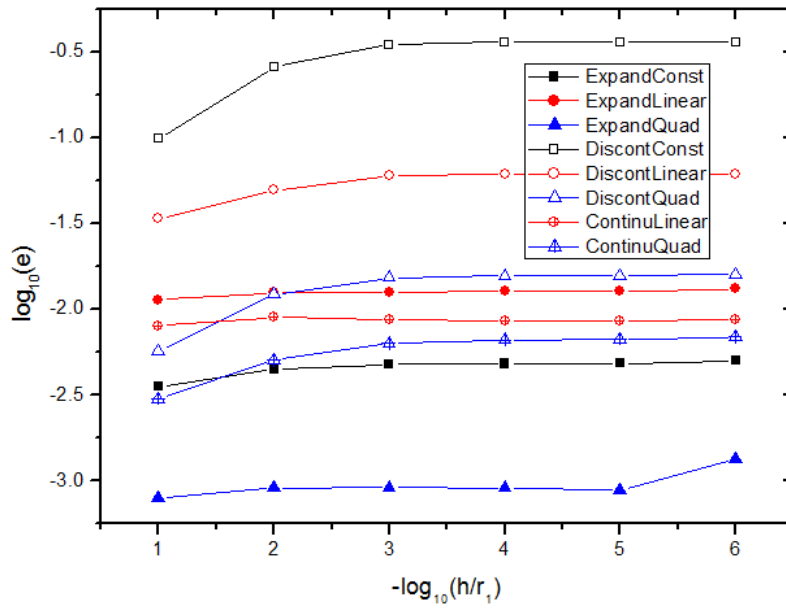


Fig. 8. Relative errors of  $t_y$  along the inner circle for different ratios  $h/r_1$ .

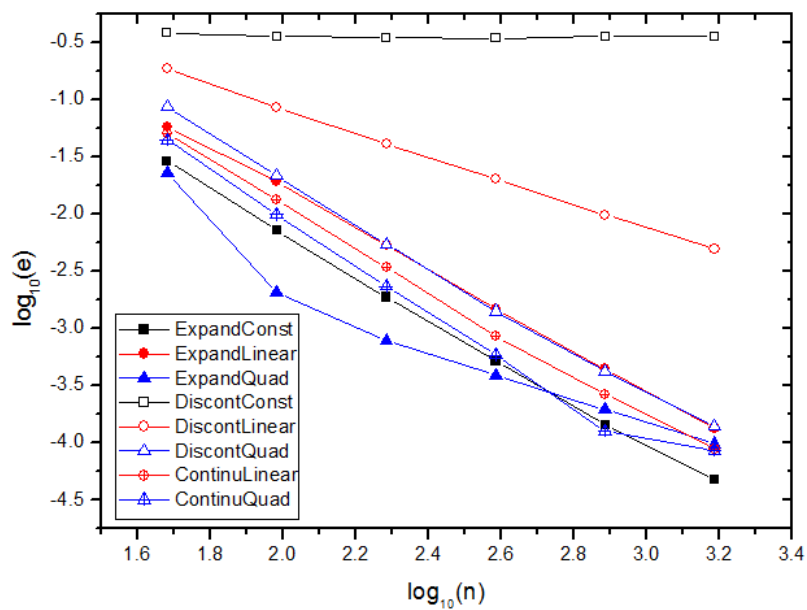


Fig. 9. Convergence rates of  $t_y$  along the inner circle for the ratios  $h/r_1 = 10^{-6}$ .

Fig. 8 and 9 show that as the coating thickness decreases, the numerical results by traditional constant element interpolation method become wrong and are hard to approach to the exact solution even with many source nodes. While no loss in solution accuracy by the expanding constant element interpolation methods as the thickness gets smaller.

#### 4.3 Example 3: cantilever beam problem

A cantilever beam problem is studied in this example as shown in Fig. 10. The exact solution is

$$u_x = -\frac{P}{6\bar{E}I} \left(y - \frac{h}{2}\right) \left[ (6l - 3x)x + (2 + \bar{\nu})(y^2 - 2hy) \right] \quad (28)$$

$$u_y = \frac{P}{6\bar{E}I} \left[ 3\bar{\nu}(y^2 - 2hy + \frac{1}{2}h^2)(l - x) + \frac{1}{4}(4 + 5\bar{\nu})h^2x + (l - \frac{1}{3}x)3x^2 \right] \quad (29)$$

where

$$I = \frac{h^3}{12} \quad (30)$$

$$\bar{E} = \begin{cases} E & \text{for plane stress} \\ E/(1 - \nu^2) & \text{for plane strain} \end{cases} \quad (31)$$

$$\bar{\nu} = \begin{cases} \nu & \text{for plane stress} \\ \nu/(1 - \nu) & \text{for plane strain} \end{cases} \quad (32)$$

The problem is solved for the plane strain case with  $P=1\text{Pa}$ ,  $E=1.1 \times 10^5\text{Pa}$ ,  $\nu=0.25$ ,  $h=1$  and  $l=100$ . Only one constant element is used on the edge  $BC$  in the proposed method and traditional method. Quadratic element is used on other edges. The numerical results of  $u_y$  along the edge  $AB$  (from  $(0, 0)$  to  $(100, 0)$ ), together with the exact solution are shown in Fig. 11. **‘ExpandQuad67’ and ‘ExpandQuad127’ stand for the numerical results by the proposed method with 67 nodes and 127 nodes, respectively.** A convergence study of  $u_y$  along the edge  $BC$  is carried out in Fig. 12.

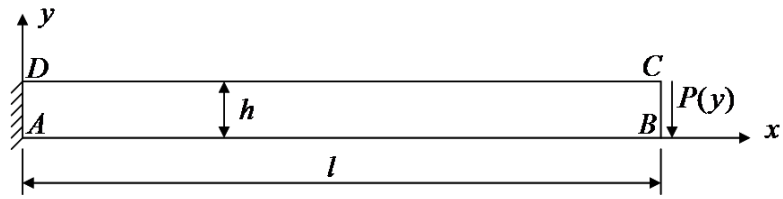


Fig. 10. Cantilever beam problem

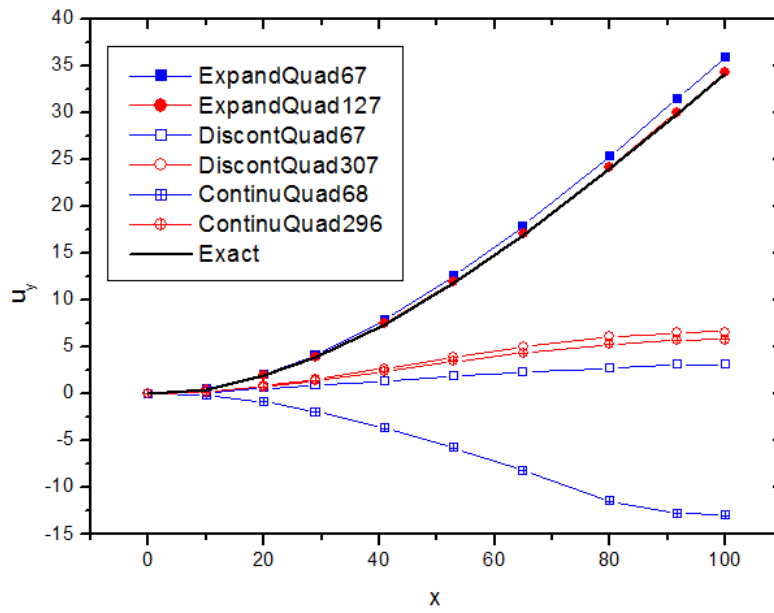


Fig. 11.  $u_y$  along the edge  $AB$  (from  $(0, 0)$  to  $(100, 0)$ ).

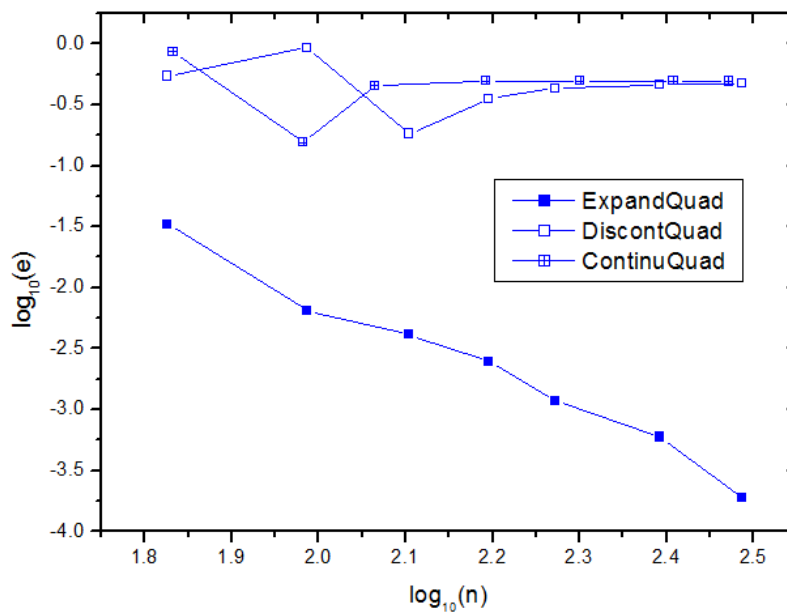
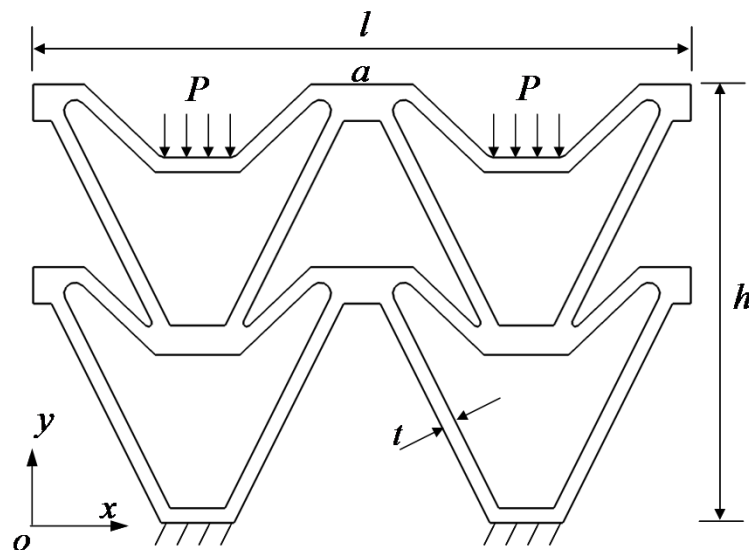


Fig. 12. Convergence rates of  $u_y$  along the edge  $BC$ .

As shown in Fig. 11, when using only one constant element on the edge  $BC$ , the numerical results by the traditional element interpolation method are completely wrong even with many source nodes. While high accuracy can be obtained by the expanding element interpolation method. From Fig. 12, it can be seen that high convergence rates is obtained by the proposed method again.

#### 4.4 Example 4: structure with negative Poisson's ratio

Some structures exhibit a negative Poisson's ratio effect under compression. In the last example, the structure with negative Poisson's ratio is considered as shown in Fig. 13. Plane strain case with  $P = 1\text{Mpa}$ ,  $E = 1000\text{MPa}$ ,  $\nu = 0.25$ ,  $h = 60$ ,  $t = 2$  and  $l = 90$  are assumed. The numerical results of  $u_y$  along the top edge  $a$ , together with the results by the FEM are shown in Fig. 14. Quadratic elements are used in both methods. 'ExpandQuad684' and 'FEM1650' denote the results by the proposed method with 684 nodes and the FEM with 1650 nodes, respectively. The numerical results by the FEM with 3232854 nodes are used as reference solution. The von Mises stress by the proposed method with 1140 nodes and the FEM with 3232854 nodes are shown in Fig. 15 and Fig. 16, respectively.



**Fig. 13.** Structure with negative Poisson's ratio.

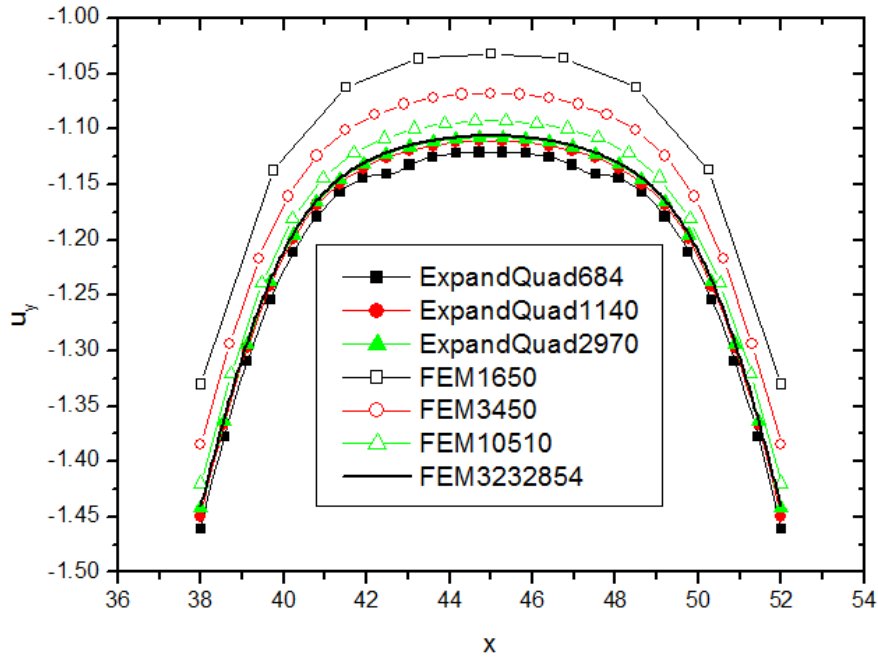


Fig. 14.  $u_y$  along the top edge  $a$ .

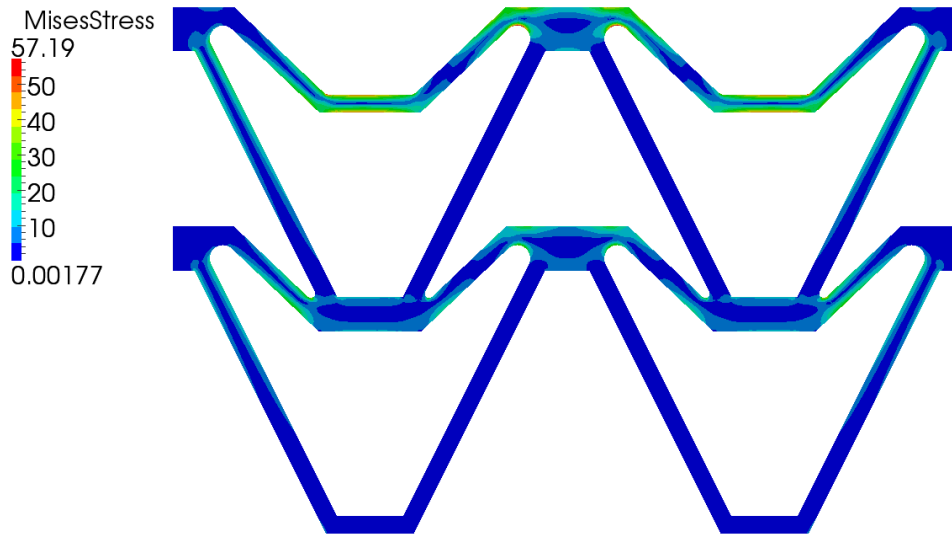
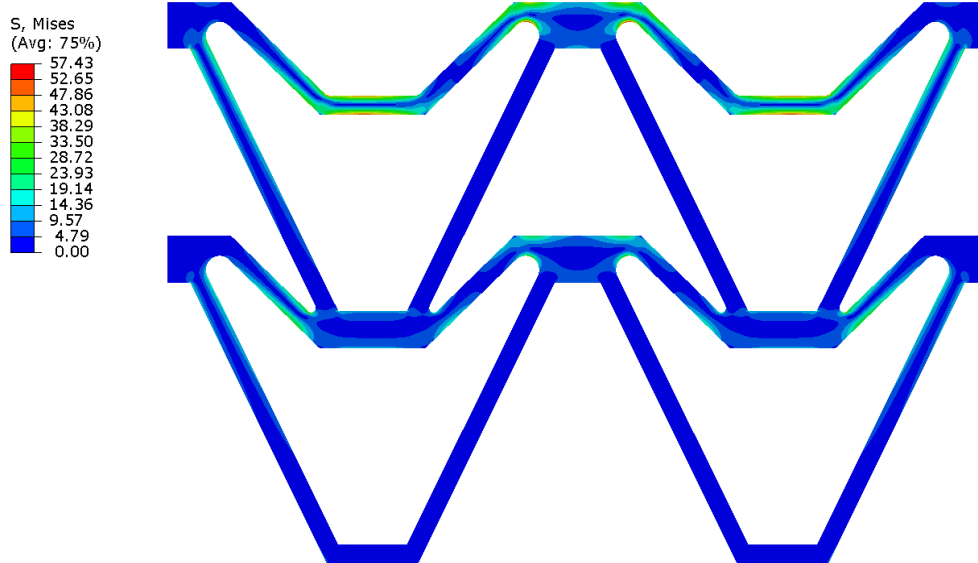


Fig. 15. Von Mises stress by the proposed method with 1140 nodes.



**Fig. 16.** Von Mises stress by the FEM with 3232854 nodes.

From Fig. 14, one can see that the numerical results of  $u_y$  by both methods approach to the reference solution as the number of node increases, but the convergence rate by the proposed method are higher than that by the FEM. As shown in Fig. 15 and 16, high level of accuracy can be obtained by the proposed method with few nodes.

## 5. Conclusions

We have applied the expanding element interpolation method to analyze thin-walled structures in this paper. The expanding element inherits the advantages of both the continuous and discontinuous elements while overcomes their disadvantages. Both continuous and discontinuous fields on the domain boundary can be accurately approximated by the expanding element interpolation method. Because the virtual nodes are not used as the source nodes, the size of the overall system of linear equations is just the same as that in the traditional discontinuous element implementation. Numerical results have demonstrated that our method has high level of accuracy and is able to analyze very slender structures with the aspect ratio up to  $10^6$ . Extension of this method for 3D cases is ongoing.

## Acknowledgment

This work was supported by National Natural Science Foundation of China under grant number 11472102 and number 11772125.

## References

- [1] Brebbia CA, Telles JCF, Wrobel LC. Boundary element techniques: theory and applications in engineering. Vol. 5. Berlin: Springer-Verlag; 1984.
- [2] Cheng AHD, Cheng DT. Heritage and early history of the boundary element method. *Engineering Analysis with Boundary Elements* 2005; 29; 268-302.
- [3] Yao ZH. A new type of high-accuracy BEM and local stress analysis of real beam, plate and shell structures. *Engineering Analysis with Boundary Elements* 2016; 65; 1-17.
- [4] Zhang JM, Lu CJ, Zhang XX, Xie GZ, Dong YQ, Li Y. An adaptive element subdivision method for evaluation of weakly singular integrals in 3D BEM. *Engineering Analysis with Boundary Elements* 2015; 51; 213-219.
- [5] Xie GZ, Zhang JM, Huang C, Lu CJ, Li GY. Calculation of nearly singular boundary element integrals in thin structures using an improved exponential transformation. *Computer Modeling in Engineering & Sciences* 2013; 94; 139-157.
- [6] Gao XW, Zhang JB, Zheng BJ, Zhang C. Element-subdivision method for evaluation of singular integrals over narrow strip boundary elements of thin-walled and slender structures. *Engineering Analysis with Boundary Elements* 2016; 66; 145-154.
- [7] Liu YJ. Analysis of shell-like structures by the boundary element method based on 3-D elasticity: formulation and verification. *International Journal for Numerical Methods in Engineering* 1998; 41; 541-558.
- [8] Luo JF, Liu YJ, Berger EJ. Analysis of two-dimensional thin structures (from micro- to nano-scales) using the boundary element method. *Computational Mechanics* 1998; 22; 404-412.
- [9] Parreira P. On the accuracy of continuous and discontinuous boundary elements. *Engineering Analysis* 1988; 5; 205-211.
- [10] Guiggiani M, Krishnasamy G, Rudolphi TJ, Rizzo FJ. A general algorithm for the numerical solution of hypersingular boundary integral equations. *Journal of Applied Mechanics* 1992; 59; 604-614.
- [11] Cisilino A. Linear and nonlinear crack growth using boundary elements. Southampton: WIT Press; 2000.
- [12] Mukhopadhyay S, Majumdar N. A study of three-dimensional edge and corner problems using the neBEM solver. *Engineering Analysis with Boundary Elements* 2009; 33; 105-119.
- [13] Tanaka M, Zhang JM, Matsumoto T. Boundary-type meshless solutions of potential problems: comparison between singular and regular formulations in hybrid BNM.

Transactions of JASCOME. Journal of Boundary Element Methods 2003; 20; 21-26.

- [14] Zhang JM, Qin XY, Han X, Li GY. A boundary face method for potential problems in three dimensions. International Journal for Numerical Methods in Engineering 2009; 80; 320-337.
- [15] Zhou HL, Niu ZR, Cheng CZ, Guan ZW. Analytical integral algorithm applied to boundary layer effect and thin body effect in BEM for anisotropic potential problems. Computers & structures 2008; 86; 1656-1671.
- [16] Xie GZ, Zhang JM, Qin XY, Li GY. New variable transformations for evaluating nearly singular integrals in 2D boundary element method. Engineering Analysis with Boundary Elements 2011; 35; 811-817.
- [17] Xie GZ, Zhang JM, Dong YQ, Huang C, Li GY. An improved exponential transformation for nearly singular boundary element integrals in elasticity problems. International Journal of Solids & Structures 2014; 51; 1322-1329.
- [18] Qin XY, Zhang JM, Xie GZ, Zhou FL, Li GY. A general algorithm for the numerical evaluation of nearly singular integrals on 3D boundary element. Journal of Computational & Applied Mathematics 2011; 235; 4174-4186.
- [19] Ma H, Kamiya N. Distance transformation for the numerical evaluation of near singular boundary integrals with various kernels in boundary element method. Engineering Analysis with Boundary Elements 2002; 26; 329-339.
- [20] Johnston BM, Johnston PR, Elliott D. A sinh transformation for evaluating two-dimensional nearly singular boundary element integrals. International Journal for Numerical Methods in Engineering 2007; 69; 1460-1479.
- [21] Johnston BM, Johnston PR, Elliott D. A new method for the numerical evaluation of nearly singular integrals on triangular elements in the 3D boundary element method. Journal of Computational & Applied Mathematics 2013; 245; 148-161.
- [22] Gu Y, Chen W, Zhang C. Stress analysis for thin multilayered coating systems using a sinh transformed boundary element method. International Journal of Solids and Structures, 2013; 50; 3460-3471.